Tracking shallow chemical gradients by actin-driven wandering of the polarization site

Jayme M. Dyer, Natasha S. Savage, Meng Jin, Trevin R. Zyla, Timothy C. Elston, and Daniel J. Lew

Supplementary Figures

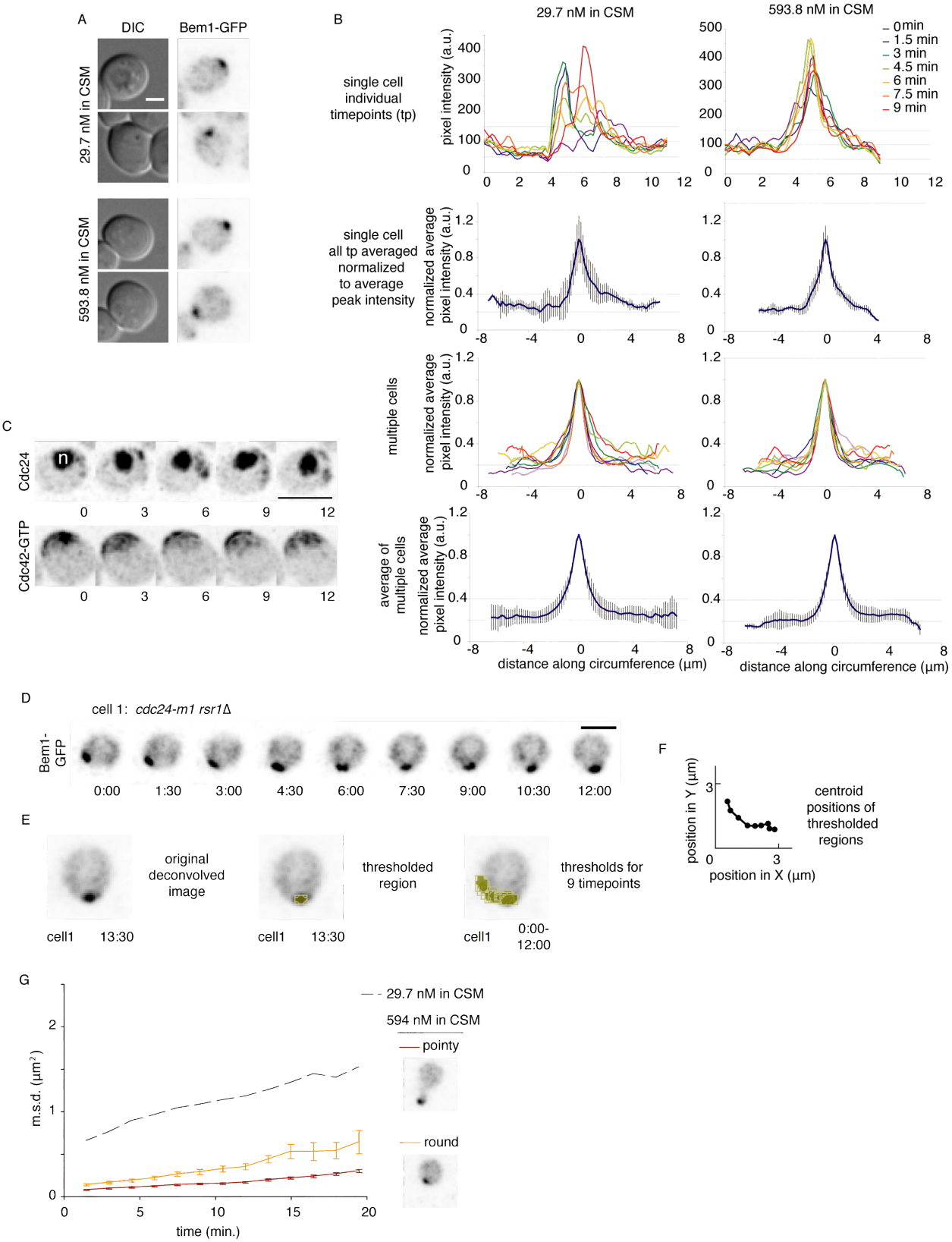

Figure S1. Polarity protein distribution and polarity patch tracking; related to Fig. 1.
A) DIC and deconvolved, inverted maximum projections of Bem1-GFP in cells treated for 2.5 h with the indicated α-factor concentrations. Cells were imaged shortly after polarizing so that polarity patches would not be affected by subsequent changes in cell morphology. Bar, 2 μm. **B) Determining Bem1-GFP distribution.** To determine the peak shape of polarized Bem1-GFP, a linescan was drawn around the perimeter of each cell in a single plane using Metamorph Software (Universal Imaging, Silver Spring, MD). Maximum fluorescence pixel intensities from a 3-pixel wide linescan (.1558μm/pixel) were reported for further analysis. Top row: Linescans from an individual cell (DLY10065) cortex were measured every 1.5 min for 9 min. At low pheromone concentration the peak wandered. Second row: the individual linescans were aligned according to peak position (peak at 0 μm) and pixel intensities were normalized at every position to the mean peak pixel intensity (set to 1, bars = standard deviation). Third row: mean values for each circumferential position are plotted. Each color shows mean values from one cell. Bottom row: the mean linescans from 8 cells were averaged (error bars = standard deviation). The resulting averages were plotted in Fig. 1B. *RSR1* and *rsr1*Δ cells exhibited similar polarity protein distributions, and 4 cells of each genotype were averaged for each pheromone concentration. **C) Cdc24-GFP and Cdc42-GTP wander in sub-saturating pheromone.** MAT**a** *bar1* cells harboring Cdc24-GFP (DLY15678) or Gic2(1-208)-tdTomato (DLY15643, a reporter of Cdc42-GTP) were pre-treated for 1 h and then imaged in 27 nM α-factor in CSM. Cdc24 is concentrated in the nucleus ("n") as well as at the cortex [1]. Time, min. Bar, 5 μm. **D-E) Tracking polarity patch wandering. D)** Montage showing Bem1-GFP wandering in a *cdc24-m1 rsr1*Δ cell (DLY11638). Time, min:s. Bar, 5 μm. Images are deconvolved, inverted maximum projections. **E)** A threshold is applied to the timelapse that selects the polarity patch. Thresholded regions (green) include 3-D fluorescence information from a z-stack, but are displayed in 2-D overlaid on an image as in **D. F)** X,Y,Z-coordinates are determined for the centroid of the thresholded region at each timepoint, yielding a patch trajectory. Positional coordinates are normalized to a stable fiduciary marker ("origin"). **G) Patch wandering at high concentrations of pheromone is slightly restricted by pointy shmoo morphology.** M.s.d. (as in Fig. 1F) for Bem1-GFP in WT cells (DLY10065) before ("round") and after ("pointy") projection formation in 594 nM α-factor. M.s.d. for cells in 29.7 nM α-factor (dashed line) is shown for comparison (identical to Fig. 2C: *RSR1*, 29.7 nM).

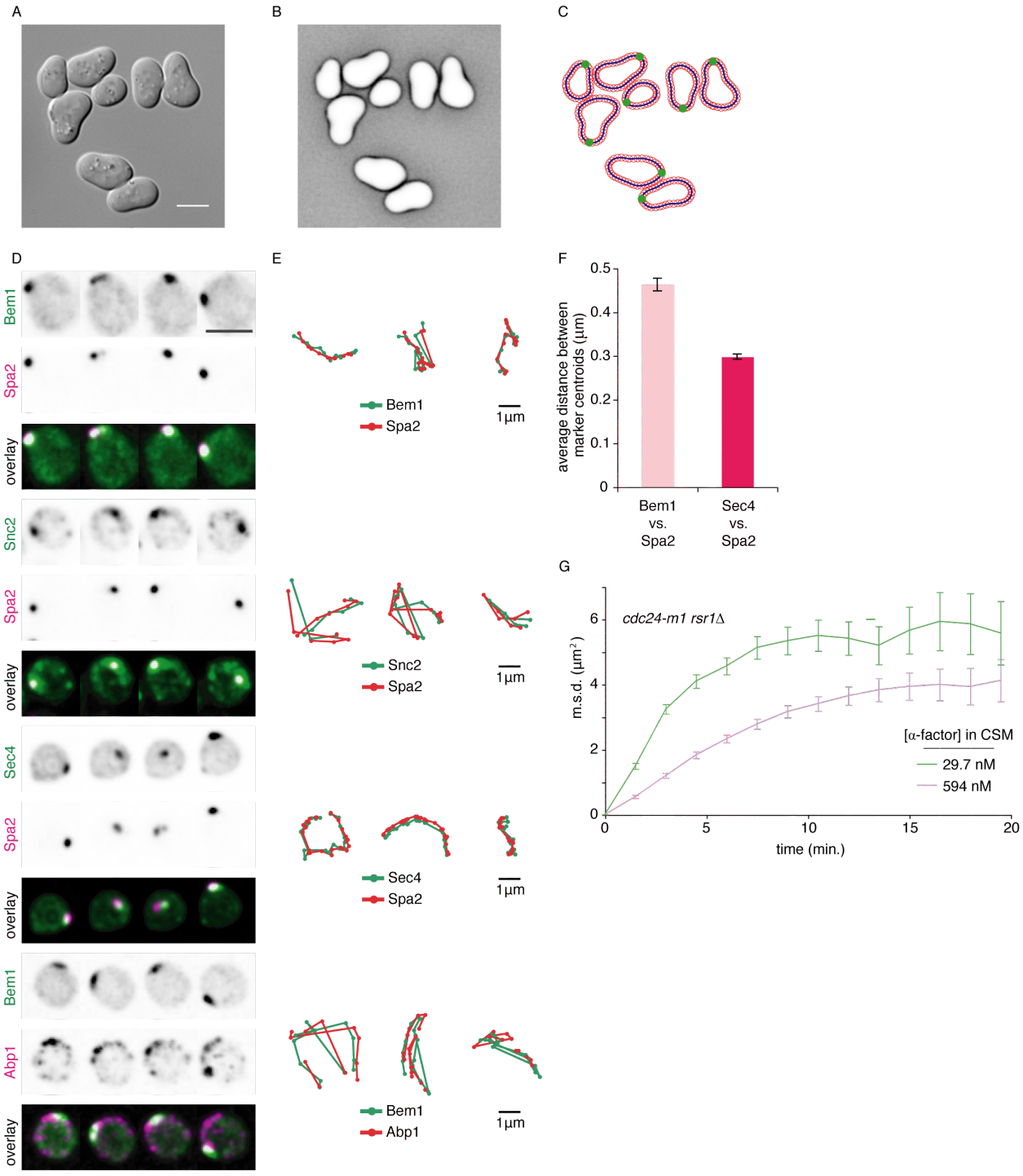
A
B
C
D
Bem1
Spa2
overlay
Snc2
Spa2
overlay
Sec4
Spa2
overlay
Bem1
Abp1
overlay
E
Bem1
Spa2
1 µm
Snc2
Spa2
1 µm
Sec4
Spa2
1 µm
Bem1
Abp1
1 µm
F
average distance between marker centroids (µm)
0.5
0.4
0.3
0.2
0.1
0
Bem1 vs. Spa2
Sec4 vs. Spa2
G
cdc24-m1 rsr1Δ
m.s.d. (µm²)
6
4
2
0
0
5
10
15
20
time (min.)
[α-factor] in CSM
29.7 nM
594 nM

Figure S2. Determination of maximum curvature and characteristics of patch wandering in *cdc24-m1 rsr1*Δ cells; related to Fig. 2.

A) DIC images of cells (DLY10065) after 2.5 h treatment with 6 nM pheromone in YEPD at 30°C. Bar, 5 μm. **B)** The cells were mixed with 20 μg/mL sulforhodamine 101 (Sigma-Aldrich, St. Louis, MO) before imaging to highlight cell boundaries. Fluorescence images were acquired over 20 z-planes with 0.24 μm steps. After deconvolution, a medial plane was selected (as shown). **C)** Smooth cell contours were obtained from a single deconvolved image (as in B) using a cubic smoothing spline routine (MATLAB 7.6). To reduce fitting error, each cell boundary was subdivided into four overlapping segments and each was fitted with a smooth contour. Curvature was calculated for every point along the curve (red dots), using the formula,

$$k_i = \frac{\left|y_i''\right|}{(1+(y_i')^2)^{3/2}}$$

Where k_i is the curvature of the i^{th} point on a smoothed contour, y'_i and y''_i are the first and second derivative of the i^{th} point on that smoothed contour. The maximum curvature value (green dot) for each cell was reported in Fig. 2B. **D)** Exocytic vesicles (marked by the Rab-family GTPase Sec4 or the v-SNARE Snc2) and nascent endocytic vesicles (marked by the actin-binding protein Abp1) roughly co-localize with the polarity proteins Bem1 and Spa2 in *cdc24-m1 rsr1*Δ cells. Frames from two-color movies of strains carrying the indicated pairs of red/green fluorescently tagged proteins (from top to bottom, DLY11638, DLY12009, DLY12037, and DLY11306). Images are deconvolved, inverted maximum projections, except overlays (GFP = green, mCherry = magenta). Bar: 5μm. **E)** All markers wander more or less together. Two-color centroid tracks for the indicated probes from the same movies in D. **F)** The average distance between marker centroids was calculated for Bem1-GFP/Spa2-mCherry and GFP-Sec4/Spa2-mCherry pairs in *cdc24-m1 rsr1*Δ cells (as in **D**). The Bem1-GFP peak is ~1μm in diameter (Fig. 1B) so an average distance of 0.45μm between patch centroids leaves considerable overlap between Bem1 and Spa2 patches. **G)** "Unconstrained" patch wandering is still somewhat sensitive to pheromone concentration. M.s.d. of Bem1-GFP in *cdc24-m1 rsr1*Δ cells (DLY11638) treated with the indicated concentrations of pheromone.

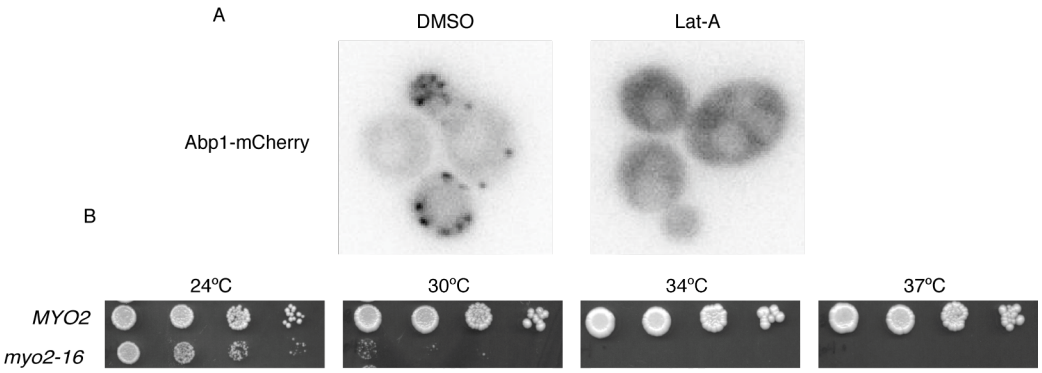

Figure S3. Efficacy of Lat A and the *myo2-16* mutation; related to Fig. 3.
A) Lat A dismantles detectable actin patches. For experiments involving Lat-A, cells either expressed Abp1-mCherry (actin patch marker; DLY11306, Fig. 3D) or cells expressing Abp1-mCherry were mixed with cells of interest (DLY11785, Fig. 3E-G). DMSO: control. Delocalization of Abp1-mCherry in cells treated with 200 µM Lat-A demonstrates the efficacy of the treatment. **B)** 34°C is a restrictive temperature for growth of *myo2-16* (DLY12404) used in Fig. 3H. Wild-type control: DLY11638. $10 - 10^4$ cells were spotted onto YEPD plates and incubated at the indicated temperatures for 2 d.

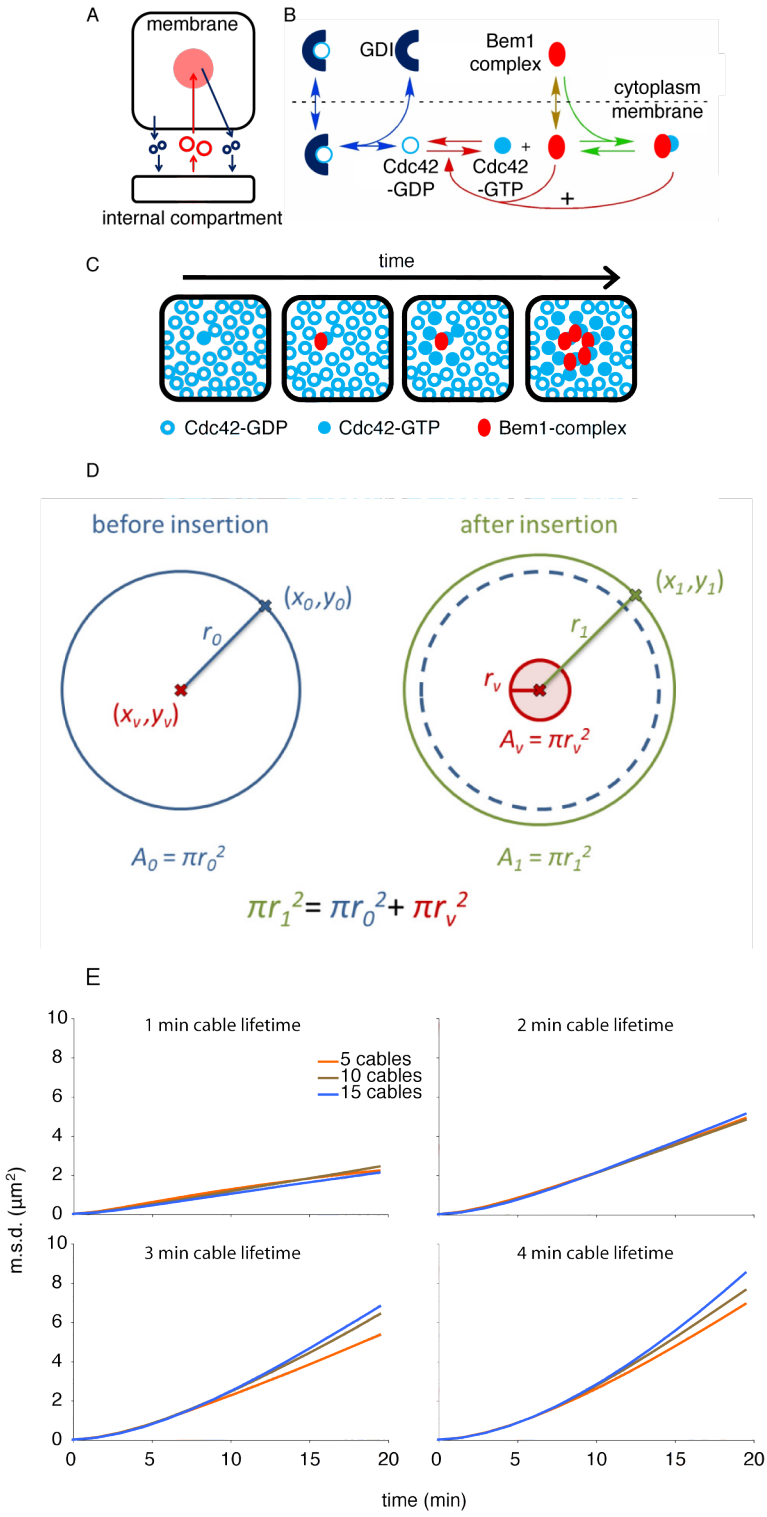
A
membrane
internal compartment
B
GDI
Bem1
complex
cytoplasm
membrane
Cdc42
-GDP
Cdc42
-GTP
+
+
C
time
Cdc42-GDP
Cdc42-GTP
Bem1-complex
D
before insertion
after insertion
(x_0,y_0)
r_0
(x_v,y_v)
(x_1,y_1)
r_1
r_v
$A_v = \pi r_v^2$
$A_0 = \pi r_0^2$
$A_1 = \pi r_1^2$
$\pi r_1^2 = \pi r_0^2 + \pi r_v^2$
E
1 min cable lifetime
2 min cable lifetime
3 min cable lifetime
4 min cable lifetime
5 cables
10 cables
15 cables
m.s.d. (μm²)
time (min)
0
2
4
6
8
10
0
5
10
15
20

Figure S4. Simulating wandering in a mathematical model; related to Fig. 4.
A-C) Schematic of the mathematical model. **A)** The model consists of three compartments, a two-dimensional plasma membrane, a well-mixed internal compartment, and a well-mixed cytoplasm. Exocytic vesicles (100 nm diameter, red) traffic from the internal compartment to the plasma membrane and endocytic vesicles (50 nm diameter, blue) traffic back to the internal compartment. **B)** Schematic representation of the reactions that describe the interactions between Cdc42, the GDI, and the Bem1 complex. **C)** Positive feedback occurs because stochastically-arising GTP-Cdc42 can recruit Bem1 complexes containing the GEF from the cytoplasm. Bound Bem1 complex promotes GTP-loading of neighboring Cdc42, leading to further recruitment of Bem1 complexes etc. **D)** Schematic of method used to calculate new concentrations in the membrane surrounding an inserted vesicle. The point (x_v, y_v) describes the coordinates of the center of the vesicle. The point at (x_0, y_0) before vesicle fusion moves to (x_1, y_1) after vesicle fusion such that the three points, (x_v, y_v), (x_0, y_0), (x_1, y_1), lie on a straight line. r_1 is the distance of point (x_1, y_1) from the center of the vesicle, r_0 is the distance of point (x_0, y_0) from the center of the vesicle, and r_v the radius of the inserted vesicle membrane. Given the area-conserving relation, $\pi r_1^2 = \pi r_0^2 + \pi r_v^2$, distances r_0 can be calculated using $r_0 = \sqrt{r_1^2 - r_v^2}$, and the coordinates (x_0, y_0) can be calculated using, $r_0 = ((x_v - x_0)^2 + (y_v - y_0)^2)^{1/2}$. **E)** Actin cable number between 5 and 15 has little effect on simulated wandering. Simulations were performed with models containing 5, 10, or 15 actin cables with lifetimes of 1,2,3, or 4 min as indicated.

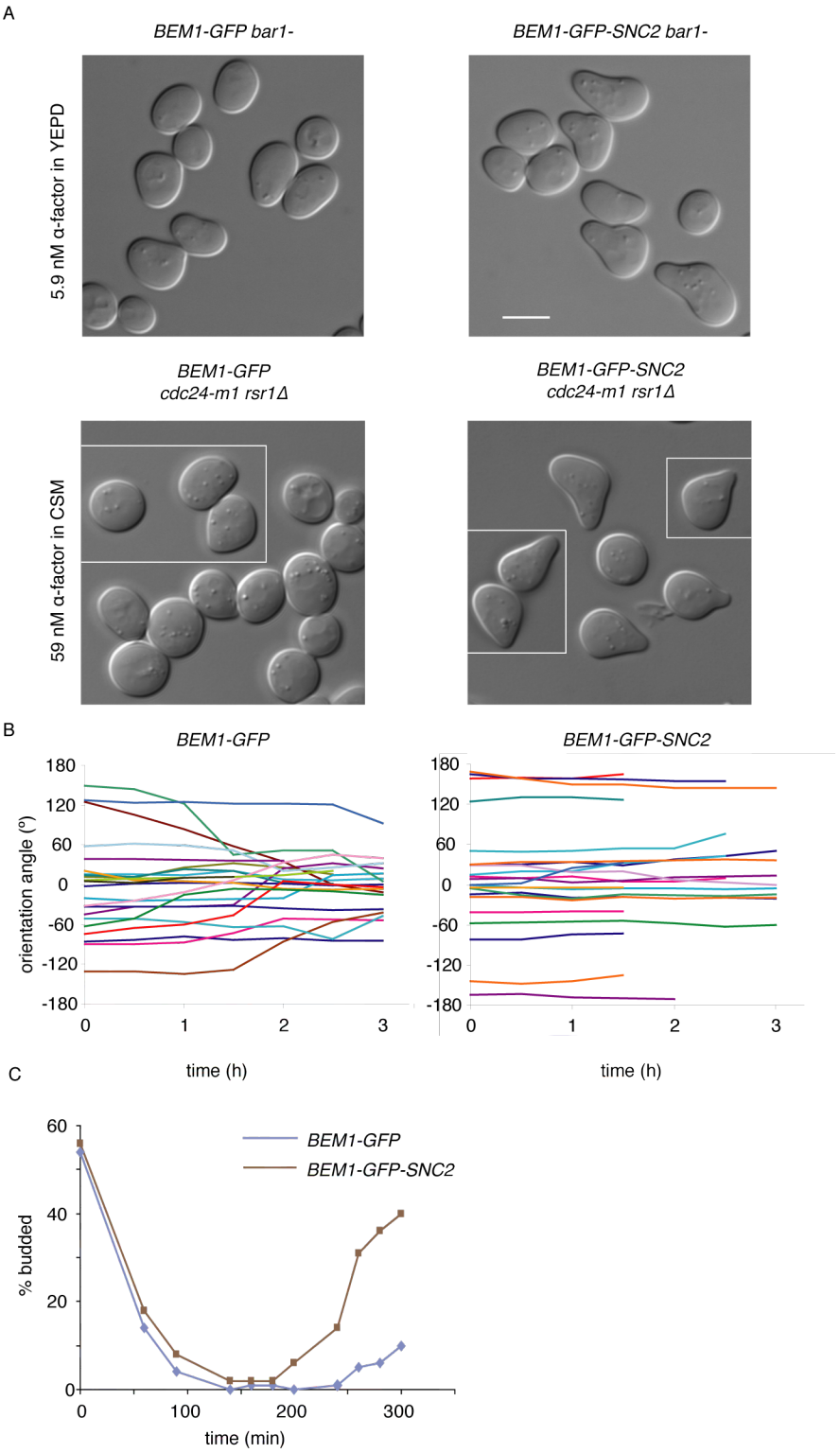
A
BEM1-GFP bar1-
BEM1-GFP-SNC2 bar1-
5.9 nM α-factor in YEPD
BEM1-GFP
cdc24-m1 rsr1Δ
BEM1-GFP-SNC2
cdc24-m1 rsr1Δ
59 nM α-factor in CSM
B
BEM1-GFP
BEM1-GFP-SNC2
orientation angle (°)
180
120
60
0
-60
-120
-180
0
1
2
3
time (h)
time (h)
C
BEM1-GFP
BEM1-GFP-SNC2
% budded
60
40
20
0
0
100
200
300
time (min)

Figure S5. Cells harboring Bem1-GFP-Snc2 make pointy projections and have impaired gradient tracking; related to Fig. 6.

A) Effect of Bem1-GFP-Snc2 on morphology of wild-type cells (DLY10065, DLY10063) treated with 5.9 nM α-factor in YEPD for 1.75 h (upper panels) and on *cdc24-m1 rsr1*Δ cells treated with 59 nM pheromone in YEPD for 3.5 h (DLY11079, DLY11099) (lower panels). Bar, 5 µm. **B)** Orientation angles (measured from DIC images) for cells of the indicated genotypes (DLY10065, DLY10063) exposed to a gradient of pheromone (as in Fig. 1E). Each line represents one cell (n=22). **C)** Bem1-GFP-Snc2 also causes accelerated recovery from cell-cycle arrest at low pheromone concentrations. Asynchronous cells (DLY10065, DLY10063) were exposed to 8.9 nM α-factor in YEPD and the budding index was scored to monitor G1 arrest and recovery. Because of the accelerated recovery, reorientation could only be followed for the first 3 h in a gradient **(B)**.

Supplementary Movie Legends

Movie S1. The polarity patch exhibits concentration-dependent wandering in uniform pheromone; related to Fig. 1. MAT**a** *bar1* cells were exposed to 594 nM α-factor **(A)** or 29.7 nM α-factor **(B-D)** in CSM for 1 h before imaging. Deconvolved, inverted, maximum projections of Bem1-GFP (**A-B,** DLY10065), Cdc24-GFP (**C,** DLY15678), and Gic2(1-208)-tdTomato (a reporter of Cdc42-GTP, **D,** DLY15643). In C, Cdc24-GFP is concentrated in the nucleus as well as the polarity patch during mating-induced G1 arrest. Time, min:s. Bar, 5 μm.

Movie S2. Cells responding to a pheromone gradient exhibit wandering patches and error correction; related to Fig. 1. MAT**a** *BEM1-GFP bar1* cells (DLY10065) were continuously exposed to a gradient of α-factor (0-12 nM in YEPD) in a microfluidics chamber. Left panels: gradient as visualized by sulforhodamine 101, a fluorescent dye included in media with high α-factor (top) to follow diffusion-mediated gradient formation. **A)** Middle panel: DIC. Right panel: deconvolved, inverted maximum projections of Bem1-GFP. **B)** Right panel: DIC. Time, h:min. Bar, 5 μm.

Movie S3. Bem1-GFP exhibits dramatic wandering in *cdc24-m1 rsr1*Δ cells; related to Fig. 2. Deconvolved, inverted maximum projections of Bem1-GFP in MAT**a** *BEM1-GFP bar1 cdc24-m1 rsr1*Δ cells (DLY11079 and DLY11638) treated with 0.3 μM α-factor in CSM. Time, min:s. Bar, 5 μm.

Movie S4. Simulated wandering of the polarity patch; related to Fig. 4. The square represents the plasma membrane, and color represents Cdc42 concentration. This simulation used the model with 5 actin cables, and 2 min average cable lifetime, which displays persistence comparable to that observed in cells (Fig. 5). For ease of comparison with the cell movies, we show snapshots at 1.5 min intervals. Exocytic events appear as dark blue patches (note that ~75 exocytic events occur between snapshots so most are not seen).

Movie S5. Bem1-GFP-Snc2 stabilizes the polarity patch in *cdc24-m1 rsr1*Δ cells; related to Fig. 6. Deconvolved, inverted maximum projections of Spa2-mCherry ("mCherry") and a) Bem1-GFP (DLY11638) or b) Bem1-GFP-Snc2 (DLY11759) ("GFP") in *cdc24-m1 rsr1*Δ cells treated with 59.4 nM α-factor in CSM. Merge shows non-inverted overlay of GFP (green) and mCherry (magenta). Time, min:s. Bar, 5 μm.

Movie S6. *BEM1-GFP-SNC2* yeast responding to a pheromone gradient; related to Fig. 6. MAT**a** *BEM1-GFP-SNC2 bar1* cells (DLY10063) were exposed to a pheromone gradient as in Movie S2. Left panel: gradient as visualized by sulforhodamine 101, highest α-factor at top. Time, h:min. Bar, 5 μm. At late times, the cells overcome the G1 arrest and bud (Fig. S5C).

Supplementary Experimental Procedures

Yeast Strains

Yeast strains used in this study are listed below. All strains are in the BF264-15Du background (*ade1 his2 leu2-3,112 trp1-1 ura3Δns*)[2], except those marked with a *, which are in the YEF473 background (*his3-Δ200 leu2-Δ1 lys2-801 trp1-Δ63 ura3-52*).

Supplementary Table 1. Yeast strains

Strain	***Relevant Genotype***
DLY10063	**a** *BEM1-GFP-SNC2:LEU2 bar1*
DLY10065	**a** *BEM1-GFP:LEU2 bar1*
DLY10066	**a** *BEM1-GFP:LEU2 rsr1::URA3 bar1*
DLY11079	**a** *BEM1-GFP:LEU2 rsr1::kan^R cdc24-m1 bar1*
DLY11094	**a** *BEM1-GFP:LEU2 cdc24-m1 bar1*
DLY11099	**a** *BEM1-GFP-SNC2:LEU2 rsr1::kan^R cdc24-m1 bar1*
DLY11306	**a** *BEM1-GFP:LEU2 ABP1-mCherry:kan^R rsr1:: kan^R cdc24-m1 bar1*
DLY11638	**a** *BEM1-GFP:LEU2 SPA2-mCherry:hyg^R rsr1:: kan^R cdc24-m1 bar1*
DLY11740	**a** *BEM1-GFP:LEU2 SPA2-mCherry:hyg^R rsr1:: kan^R bar1*
DLY11742	**a** *BEM1-GFP:LEU2 SPA2-mCherry:hyg^R bar1*
DLY11759	**a** *BEM1-GFP-SNC2:LEU2 SPA2-mCherry:hyg^R rsr1:: kan^R cdc24-m1 bar1*
DLY11785	**a**/α *ABP1-mCherry:kan^R /ABP1-mCherry:kan^R CDC3-GFP:URA3/ CDC3-GFP:URA3*
DLY12009	**a** *SPA2-mCherry:Hyg^R P$_{GAL}$-GFP-SNC2:TRP1 GAL4BD-hER-VP16:TRP1 cdc24-m1 rsr1::kan^R bar1*
DLY12037	a *SPA2-mCherry:HYG^R rsr1::KAN^R cdc24-m1 GFP-SEC4:URA3 bar1*
DLY12404	**a** *BEM1-GFP:LEU2 SPA2-mCherry:hyg^R, myo2-16:URA3 rsr1:: kan^R cdc24-m1 bar1*
DLY13898*	**a** *GFP-CDC42:URA3*
DLY14148	**a** *BEM1-GFP-SNC2:LEU2 SPA2-mCherry:hyg^R bar1*

DLY14160	**a** *BEM1-GFP:LEU2 myo4::URA3 rsr1::kan^R cdc24-m1 bar1*
DLY15643*	**a** *GIC2(1-208)-tdTomato::kan^R bar1::URA3*
DLY15678	**a** *CDC24-GFP::kan^R bar1*

The *rsr1::URA3, myo4::URA3,* and *bar1::URA3* disruptions were generated by the one-step PCR-based method [3] using pRS306 as template [4]. The *rsr1::kan^R* disruption was generated similarly using genomic DNA from the ResGen deletion collection as template.

SPA2-mCherry and *ABP1-mCherry* were generated by the PCR-based C-terminal tagging method [5] using as template pDLB2866 (*pFA6a-mCherry-ADH1t-hphMX4*) or pDLB2865 (*pFA6a-mCherry-ADH1t-kanMX6*). *P_{GAL}-GFP-SNC2* was generated similarly, using as template pDLB2326 (*pFA6a-TRP1-P_{GAL}-GFP*). A Gly-Ala-Gly linker was introduced between the *GFP* and *SNC2* open reading frames (ORFs). *CDC24-GFP* and *GIC2(1-208)-tdTomato* were generated similarly, using as template pDLB53 (pFA6a-GFP(S65T)-KanMX6) and pDLB3301 (pFA6a-tdTomato-KanMX6), respectively. A Pro-Glu-Pro linker was introduced between the *CDC24* and *GFP* ORFs. Oligonucleotides for the *GIC2(1-208)-tdTomato* transformation were designed to truncate the endogenous *GIC2* gene at nucleotide 624.

To generate the strain harboring *GFP-SEC4*, pDLB2776 (YIplac211-*GFP-SEC4*, a gift from E. Bi) was cut with *Stu*I to target integration at *URA3*. To generate the strain harboring *GFP-CDC42,* pDLB3609 (YIplac211-*pCDC42-GFP-linker-CDC42*) was cut with *Eco*RV to target integration at *URA3*. The linker in pDLB3609 is: Lys Gly Ser Cys Gly Arg Ala Pro Pro Arg Arg Leu Val His Pro [6]. Strains expressing *BEM1-GFP* and *BEM1-GFP-SNC2* at the *BEM1* locus were created as previously described [7, 8]. To generate the strain harboring *CDC3-GFP*, pDLB3139 (YIplac211-*CDC3-GFP*, a gift from E. Bi) was cut with *Spe*I to target integration at *CDC3*.

To express the hybrid transcription factor *GAL4BD-hER-VP16* [9], plasmid pPP1557 (pRS304-*P_{ADH1}-GAL4BD-hER-VP16*, [10]) was digested with *Sna*BI to target integration at *TRP1*.

To replace *MYO2* with *myo2-16*, plasmid pDLB2006 (pRS306-*myo2-16*, a gift from A. Bretscher) was digested with *Spe*I to target integration at *MYO2* [11].

To replace *CDC24* with *cdc24-m1*, the *CDC24* promoter and full-length *cdc24-m1* ORF was excised from pDLB3156 (pRS414-*cdc24-m1*, a gift from R. Arkowitz) using *Apa*I and *Spe*I and transformed into DLY5682 (MAT**a** *cdc24-4 rsr1::KAN^R bar1*). Transformants were selected on YEPD at 37°C to select for replacement of the temperature-sensitive *cdc24-4* allele. Replacement of *cdc24-4* (G168D) with *cdc24-m1* (S189F) was confirmed by sequence analysis. Unmarked *cdc24-m1* was crossed into subsequent strains.

Computational Methods

Simulating diffusion on the surface of a sphere

Diffusion on a plane yields $\langle d^2 \rangle = 4Dt$, where $\langle d^2 \rangle$ is the mean squared displacement (msd) from the origin, D is the effective diffusion coefficient, and t is time. However, due to the geometrical constraint imposed by the surface of a sphere with radius r, $\langle d^2 \rangle$ will deviate from this relation and eventually plateau at $\langle d^2 \rangle = 2r^2$. To see why this is the case, consider that a particle diffusing from an arbitrary origin will, after a long time, reside with equal probability at any point on the sphere. For a sphere with center (0,0,0), all points on the surface are described by $(r\sin\theta\cos\phi, r\sin\theta\sin\phi, r\cos\theta)$, where $0 \le \theta \le \pi$ and $0 \le \phi \le 2\pi$. The squared displacement, d^2, of any point on the surface from an origin positioned at $(0,0,r)$ is,

$$d^2 = (0 - r\sin\theta\cos\phi)^2 + (0 - r\sin\theta\sin\phi)^2 + (r - r\cos\theta)^2 = 2r^2(1 - \cos\theta)$$

Thus the expected msd $\langle d^2 \rangle$ is,

$$\langle d^2 \rangle = \frac{\int_0^\pi 2r^2(1-\cos\theta)\,d\theta}{\int_0^\pi d\theta} = 2r^2$$

To simulate diffusion on a sphere, we first estimated an appropriate diffusion coefficient to match the wandering patch data. Assuming that the initial displacement is not significantly constrained by the cell geometry, the msd at the first timepoint (1.5 min) was fit to $\langle d^2 \rangle = 4Dt$ to extract the diffusion coefficient, with a small modification to account for the curvature of the cell surface. We then solved the diffusion equation on the surface of a sphere (radius R=2 μm to match the mean cell size) to compute the time-dependent probability density for a Brownian particle started at (0,0,R). This distribution and the squared distance of each grid point on the discretized sphere from the origin were used to calculate the msd using the formula,

$$\langle d^2 \rangle = \sum_{i \in S} d_i^2 p_i$$

where *i* are the grid points on the surface *S*, p_i is the value of the probability distribution and d_i^2 is the squared distance at grid point *i*.

Simulating actin-independent positive feedback

We used the mathematical model developed by Goryachev and Pokhilko [12] to model actin-independent polarization due to Cdc42, the Bem1 complex, and the GDI. This model consists of two compartments, a two-dimensional plasma membrane and a well-mixed cytoplasm, and uses mass-action reaction kinetics to describe the interactions between these three proteins

and diffusion to describe their movement. At the membrane, all species diffuse with diffusion constant D_m=0.0025 μm^2/s. The behaviors of the different molecular entities are as follows:

Cdc42: Membrane-associated Cdc42 can be either GDP-bound (denoted Cdc42D) or GTP-bound (Cdc42T). Cdc42 GDP/GTP exchange is catalyzed by the Bem1 complex at the membrane, and GAP-stimulated Cdc42 GTP hydrolysis is described by a first-order rate constant.

Bem1 complex: Denoted BemGEF at the membrane or BemGEFc when cytoplasmic, the Bem1 complex exchanges between membrane and cytoplasm, and can bind reversibly to GTP-Cdc42 at the membrane, forming the complex denoted BemGEF42. GTP-Cdc42 can also bind cytoplasmic Bem1 complex. BemGEF42 is assumed to have 2-fold higher GEF activity than the unbound BemGEF.

GDI: The GDI is a cytoplasmic protein (denoted GDIc) that can bind GDP-Cdc42 at the membrane, generating the complex denoted GDI42. This complex can exchange between membrane and cytoplasm (and is denoted GDI42c when cytoplasmic).

The equations governing the behavior of these species are as follows (Fig. S4B):

$$\frac{\partial}{\partial t}Cdc42T = (k_{2a}BemGEF + k_3BemGEF42)\cdot Cdc42D - k_{2b}Cdc42T - k_{4a}BemGEF\cdot Cdc42T + k_{4b}BemGEF42 - k_7BemGEFc\cdot Cdc42T + D_m\Delta Cdc42T$$

$$\frac{\partial}{\partial t}BemGEF42 = k_{4a}BemGEF\cdot Cdc42T - k_{4b}BemGEF42 + k_7BemGEFc\cdot Cdc42T + D_m\Delta BemGEF42$$

$$\frac{\partial}{\partial t}BemGEF = k_{1a}BemGEFc - k_{1b}BemGEF - k_{4a}BemGEF\cdot Cdc42T + k_{4b}BemGEF42 + D_m\Delta BemGEF$$

$$\frac{\partial}{\partial t}BemGEFc = \eta(k_{1b}BemGEF - (k_{1a} + k_7Cdc42T)\cdot BemGEFc) + D_c\Delta BemGEFc$$

$$\frac{\partial}{\partial t}Cdc42D = k_{2b}Cdc42T - (k_{2a}BemGEF + k_3BemGEF42)\cdot Cdc42D + k_{6b}GDI42 - k_{6a}GDIc\cdot Cdc42D + D_m\Delta Cdc42D$$

$$\frac{\partial}{\partial t}GDI42 = k_{6a}GDIc\cdot Cdc42D - k_{6b}GDI42 + k_{5a}GDI42c - k_{5b}GDI42 + D_m\Delta GDI42$$

$$\frac{\partial}{\partial t}GDI42c = \eta(k_{5b}GDI42 - k_{5a}GDI42c) + D_c\Delta GDI42c$$

$$\frac{\partial}{\partial t}GDIc = \eta(k_{6b}GDI42 - k_{6a}GDIc\cdot Cdc42D) + D_c\Delta GDIc$$

The plasma membrane is modeled as a discretized surface, with surface area equal to that of a 5 μm diameter sphere. Periodic boundary conditions are used to avoid edge effects, i.e. diffusion is on a torus.

In order to allow for the incorporation of vesicle traffic, the system has an additional internal compartment, absent in the Goryachev model, which represents the endomembrane system relevant to Cdc42 recycling (Fig. S4A)[13]. The internal compartment contains no GEF, so all Cdc42 in this compartment is GDP bound, and it is assumed that the GDI can exchange GDP-Cdc42 between the cytoplasm and the internal compartment in exactly the same way that it exchanges GDP-Cdc42 between the cytoplasm and the plasma membrane. Thus, the concentration of Cdc42 in the internal compartment is similar to that in the plasma membrane at locations distant from the polarity peak.

Generating different polarity peaks

Simulations are initiated with a small transient spike of GTP-Cdc42 in the middle of the plasma membrane, which evolves to a polarized steady state. The Cdc42 profile in Fig. 3C was obtained using parameter values based on fitting FRAP data as described in [13]. Larger and smaller Cdc42 peaks (Fig. 4A, left) were obtained by varying the GAP reaction rate constant k_{2b}; broader and narrower Cdc42 peaks (Fig. 4A, middle) were obtained by varying the diffusion constant D_m; and similar-shaped peaks with different dynamics (Fig. 4A, right) were obtained by varying the diffusion constant and multiplying all reaction rate constants by a factor that returns the distribution to the original shape/size. FRAP simulations were performed as described [13].

Previous modeling studies assumed a total cellular Cdc42 concentration of 5 μM [12, 13], but recent quantitative data from fluorescence correlation spectroscopy suggest that Cdc42 is only present at 1 μM (Das et al. 2012). To model a realistic Cdc42 peak, we reduced the Cdc42 and GDI concentrations in the model accordingly. Then, model parameters were adjusted to obtain a peak that matched the profile measured for GFP-Cdc42 by fluorescence microscopy (Fig. 4B). With these parameters (Supplementary Table 2), the peak displayed a FRAP $t_{1/2}$ of 2.6 s (comparable to the observed Cdc42 FRAP: Fig. 3F), and approximately 7.3% of the cellular Cdc42 was present in the peak (consistent with imaging results).

Supplementary Table 2. Parameter values for the reaction-diffusion model

Description		**Parameter**		Units
*Cdc*42*D* + *BemGEF*	→*Cdc*42*T* + *BemGEF*	k_{2a}	0.16	$\mu M^{-1}\ s^{-1}$
*Cdc*42*D* + *BemGEF*42	→*Cdc*42*T* + *BemGEF*42	k_3	0.35	$\mu M^{-1}\ s^{-1}$
*Cdc*42*T*	→*Cdc*42*D*	k_{2b}	0.63	s^{-1}
*Cdc*42*D* + *GDIc*	→*GDI*42	k_{6a}	240	$\mu M^{-1}\ s^{-1}$
*GDI*42	→*Cdc*42*D* + *GDIc*	k_{6b}	80	s^{-1}
*GDI*42	→ *GDI*42*c*	k_{5b}	20.8	s^{-1}
*GDI*42*c*	→ *GDI*42	k_{5a}	144	s^{-1}

Cdc42T + BemGEF	→*BemGEF42*	k_{4a}	10	$\mu M^{-1}\ s^{-1}$
Cdc42T + BemGEFc	→*BemGEF42*	k_7	10	$\mu M^{-1}\ s^{-1}$
BemGEF42	→ *Cdc42T + BemGEF*	k_{4b}	10	s^{-1}
BemGEFc	→*BemGEF*	k_{1a}	10	s^{-1}
BemGEF	→*BemGEFc*	k_{1b}	10	s^{-1}
	Volume ratio	η	0.01	
	Diffusion constant (membrane)	D_m	0.0045	$\mu m^2\ s^{-1}$
Total [Cdc42p]			1	μM
Total [BemGEF]			0.017	μM
Total [GDI]			1	μM

Simulating the effect of a single secretory vesicle fusion event

Secretory vesicles carry GDP-Cdc42 and GDP-Cdc42-GDI but not the Bem1 complex. The concentration of these proteins on the vesicle is unknown, but for our simulations we assume that Cdc42 undergoes 'bulk traffic': i.e. Cdc42 concentration on the vesicles is the same as in the internal compartment.

The simulated plasma membrane of a 5 μm diameter cell is discretized into 10,000 regular grid points. Therefore, a secretory vesicle with diameter 100 nm has a surface area equivalent to 4 grid points. (In the model, vesicle size is a fixed fraction of cell size, so to maintain the correct vesicle size we used a 5 μm diameter cell even though haploid cells were generally a bit smaller). To simulate a vesicle fusion event while retaining the same regular grid, the following steps are taken:

First, four grid points (a 2x2 square) are designated as the inserted vesicle membrane immediately after the fusion event: the protein concentrations at these points will be set equal to those on the vesicle. The center of the vesicle insertion is considered to be the center of the inserted 2x2 square.

We assume that points on the plasma membrane are shifted radially outwards as a result of vesicle fusion (Fig. S4D). Using conservation of area (see [13] for a full description), we can then calculate the instantaneous protein distribution at all remaining grid points immediately after vesicle fusion. We re-size the area assigned to each grid point to reflect the fact that we represented the same membrane area with 10,000 grid points before fusion but only 9,996 grid points after fusion (as 4 grid points were re-assigned to represent the vesicle membrane).

To calculate the distance that a single vesicle fusion event would shift a reaction-diffusion peak, we began with the polarized steady state of the reaction-diffusion system and designated a location for the vesicle fusion event. After simulating vesicle fusion as described above, we allowed the system to evolve to a new reaction-diffusion steady state. The precise position of

the peak of the distribution was estimated by interpolation using splines and the peak shift was calculated as the distance between the pre-fusion and final peak positions.

As shown in Fig. 3C and 4C, the peak shift was dependent on the location of vesicle fusion in relation to the center of the peak. For Fig. 4A, the location of vesicle fusion was chosen so as to maximize the peak shift. Thus, the distance from the center of the peak to the vesicle fusion site varied with the size and shape of the peak (Supplementary Table 3).

Supplementary Table 3

k2b (s^{-1}) (GAP activity)	**2.52**	**1.89**	**1.26**	**0.63**	**0.315**	**0.1575**	**0.07875**	**0.0315**
Cdc42 in the polarity patch	1.44	1.85	2.57	4.33	7.02	10.92	16.20	25.71
peak shift (nm)	12.6	11.4	9.9	8.1	6.7	5.7	5.0	4.4
distance from vesicle to peak (μm)	0.38	0.50	0.50	0.63	0.75	0.88	1.00	1.25
D_m ($\mu m^2 s^{-1}$)	**0.0001**	**0.0003**	**0.0012**	**0.0025**	**0.0067**	**0.0109**	**0.0193**	**0.036**
peak width at half height (μm)	0.89	1.06	1.42	1.77	2.30	2.66	3.19	4.25
peak shift (nm)	14.0	11.6	9.1	8.1	6.9	6.3	5.7	5.0
distance from vesicle to peak (μm)	0.38	0.50	0.63	0.63	0.75	0.88	1.00	1.00
all reaction multiplier	**8.5**	**3.244**	**1.932**	**1**	**0.438**	**0.203**	**0.0984**	**0.0497**
D_m ($\mu m^2 s^{-1}$)	**0.0075**	**0.005**	**0.0038**	**0.0025**	**0.0013**	**0.00065**	**0.00033**	**0.00017**
peak shift (nm)	4.5	6.9	7.5	8.1	8.8	9.1	9.2	9.2
distance from vesicle to peak (μm)	0.88	0.75	0.75	0.63	0.63	0.63	0.63	0.63

Simulating wandering due to stochastic vesicle traffic

To simulate wandering due to vesicle traffic, we used the combined mathematical model of Savage et al. [13], with the following modifications:

1. The parameter set for the reaction-diffusion process (Supplementary Table 2) was changed as discussed above so as to match the polarity peak to the observed Cdc42 distribution (Fig. 4B) and dynamics (Fig. 3F).

2. The vesicle traffic rate was set so as to obtain a realistic exocytosis rate. Based on the observed rates of endocytosis in cells (~100 events/min), maintenance of plasma membrane area would require ~25 exocytic events/min (exocytic vesicles have ~4x the area of endocytic vesicles)[14]. Net growth adds another ~25 exocytic events/min (a linear approximation for cell growth given a doubling time of 90 min: cell surface area=vesicle area.25 vesicles/min.90 min),

yielding a total exocytosis rate of ~50 vesicles/min. As the important parameter for wandering is the exocytosis rate (not the endocytosis rate), we set the endocytosis rate to 200 events/min so as to maintain a constant surface area in the model cell.

3. The window represents the polarity patch: grid points containing the highest concentration of Cdc42 are designated to be in the window. The window area was set to be 2% of the total plasma membrane, so as to approximately match the dimensions of the polarity patch. Exploration of other window dimensions suggested that wandering is not very sensitive to this parameter. As in Savage et al. [13], endocytic events can happen anywhere, but they occur with 40-fold higher probability (per unit area) in the window. In simulations without actin cables, exocytic events happen with equal probability at any points within the window, but not elsewhere. A fusion site is chosen by first assigning a grid point within the window and then randomly assigning which of the four exocytic grid points will be anchored at the fusion site.

4. For simulations of actin cable-mediated traffic, we designated two new parameters: actin cable number N and actin cable lifetime τ. We assume that cables attach, with the rate of one per second (as long as the cable number is less than N), to any grid point within the window with equal probability, and detach with probability $1/\tau$ min^{-1}. When vesicle fusion events occur, they happen with equal probability at any of the grid points at which a cable is currently attached, but not elsewhere.

To obtain msd plots and persistence estimates from simulations, 10 independent 150 min simulations were performed for each condition. To match the image analysis used for cells, simulated polarity patch centroid positions were recorded at 90 second intervals and defined as the center of the smallest box containing the thresholded patch. Because of the larger diameter of the model cell (see above) compared to the haploid yeast, msd values plateaued at higher msd for simulations than they did for cells for cells.

Simulating the effect of Bem1-Snc2

To simulate the effects of concentrating Bem1 on secretory vesicles (Fig. 6A), we added a new species to the model, representing Bem1-GFP-Snc2. The abundance and GEF activity of this protein was set equal to the abundance and activity of BemGEF, but instead of exchanging between the cytoplasm and the plasma membrane, the new species traffics between the plasma membrane and the internal compartment by endocytosis and exocytosis. As previously described for v-SNAREs [14], the new species is actively concentrated into endocytic vesicles from the plasma membrane and into exocytic vesicles from the internal compartment. Following vesicle fusion, this membrane-tethered species behaves just like the normal Bem1 complex (reversibly binds GTP-Cdc42, catalyzes GDP/GTP exchange, diffuses) except that it cannot move to the cytoplasm.

Supplementary References

1. Nern, A., and Arkowitz, R.A. (2000). Nucleocytoplasmic shuttling of the Cdc42p exchange factor Cdc24p. J Cell Biol *148*, 1115-1122.

2. Richardson, H.E., Wittenberg, C., Cross, F., and Reed, S.I. (1989). An essential G1 function for cyclin-like proteins in yeast. Cell *59*, 1127-1133.

3. Baudin, A., Ozier-Kalogeropoulos, O., Denouel, A., Lacroute, F., and Cullin, C. (1993). A simple and efficient method for direct gene deletion in *Saccharomyces cerevisiae*. Nucleic Acids Res. *21*, 3329-3330.

4. Sikorski, R.S., and Hieter, P. (1989). A system of shuttle vectors and yeast host strains designed for efficient manipulation of DNA in *Saccharomyces cerevisiae*. Genetics *122*, 19-27.

5. Longtine, M.S., McKenzie III, A., DeMarini, D.J., Shah, N.G., Wach, A., Brachat, A., Philippsen, P., and Pringle, J.R. (1998). Additional modules for versatile and economical PCR-based gene deletion and modification in *Saccharomyces cerevisiae*. Yeast *14*, 953-961.

6. Köhli, M., Galati, V., Boudier, K., Roberson, R.W., and Philippsen, P. (2008). Growth-speed-correlated localization of exocyst and polarisome components in growth zones of Ashbya gossypii hyphal tips. Journal of Cell Science *121*, 3878-3889.

7. Kozubowski, L., Saito, K., Johnson, J.M., Howell, A.S., Zyla, T.R., and Lew, D.J. (2008). Symmetry-Breaking Polarization Driven by a Cdc42p GEF-PAK Complex. Current Biology *18*, 1719-1726.

8. Howell, A.S., Savage, N.S., Johnson, S.A., Bose, I., Wagner, A.W., Zyla, T.R., Nijhout, H.F., Reed, M.C., Goryachev, A.B., and Lew, D.J. (2009). Singularity in Polarization: Rewiring Yeast Cells to Make Two Buds. Cell *139*, 731-743.

9. Louvion, J.F., Havaux-Copf, B., and Picard, D. (1993). Fusion of GAL4-VP16 to a steroid-binding domain provides a tool for gratuitous induction of galactose-responsive genes in yeast. Gene *131*, 129-134.

10. Takahashi, S., and Pryciak, P.M. (2008). Membrane localization of scaffold proteins promotes graded signaling in the yeast MAP kinase cascade. Curr Biol *18*, 1184-1191.

11. Schott, D., Ho, J., Pruyne, D., and Bretscher, A. (1999). The COOH-Terminal Domain of Myo2p, a Yeast Myosin V, Has a Direct Role in Secretory Vesicle Targeting. J Cell Biol *147*, 791-808.

12. Goryachev, A.B., and Pokhilko, A.V. (2008). Dynamics of Cdc42 network embodies a Turing-type mechanism of yeast cell polarity. FEBS Lett *582*, 1437-1443.

13. Savage, N.S., Layton, A.T., and Lew, D.J. (2012). Mechanistic mathematical model of polarity in yeast. Molecular Biology of the Cell *23*, 1998-2013.

14. Layton, A.T., Savage, N.S., Howell, A.S., Caroll, S.Y., Drubin, D., and Lew, D.J. (2011). Modeling vesicle traffic reveals unexpected consequences for Cdc42p-mediated polarity establishment. Curr Biol *21*, 184-194.